Applied Surface Science 631 (2023) 157547

Contents lists available at ScienceDirect

Applied Surface Science

journal homepage: www.elsevier.com/locate/apsusc

Full Length Article

From DFT investigations of oxygen-implanted molybdenum disulfide to temperature-induced stabilization of MoS_2/MoO_3 heterostructure

Sylwia Kozdra [a,*], Adrianna Wójcik [a,b], Tamal Das [c], Paweł Piotr Michałowski [a]

[a] Łukasiewicz Research Network – Institute of Microelectronics and Photonics, Aleja Lotników 32/46, Warsaw 02-668, Poland
[b] Warsaw University of Technology, Faculty of Physics, Koszykowa 75, Warsaw 00-662, Poland
[c] Hylleraas Centre for Quantum Molecular Sciences, Department of Chemistry, University of Oslo, P.O. Box 1033, Blindern, N-0315 Oslo, Norway

ARTICLE INFO

Keywords:
Molybdenum disulfide
Molybdenum trioxide
Heterostructure
Density functional theory
Secondary Ion Mass Spectrometry

ABSTRACT

In this work, we study the mechanism of the implantation process of two-dimensional molybdenum disulfide. We proposed the oxidation scheme and investigated the changes in the geometry of the MoS_2 layer, as well as HOMO and LUMO orbitals location using the Density Functional Theory technique. We found that the oxygen was incorporated into the MoS_2 structure and the MoS_2/MoO_3 heterostructure was created. The effect of implantation and the presence of heterostructure was investigated in the Secondary Ion Mass Spectrometry technique with atomic-resolution depth profiles. The presence of molybdenum trioxide was confirmed using Raman spectroscopy. The successful implantation allowed to obtain a stable conductive/insulating heterostructure of MoS_2/MoO_3 with promising properties.

1. Introduction

The ability to modulate the properties of semiconductors has been a key factor in the success of two-dimensional (2D) materials. The possibility of implementing changes in their structure at the nano level opened gates for achieving materials tailored to current needs. However, to realize the potential of 2D semiconductors, a reliable and precise method of modification and analysis of their chemical structure is desired.

One of the ways of modulating the properties of 2D materials is the implantation of ions into their structure. As a result of implantation, the heterostructure with new properties is created. The extent of the implantation phenomenon depends on the energy of the implanted ions [1]. One of the advantages of using ion implantation is its versatility to introduce almost any element to the lattice of the targeted material. Ion implantation into bulk materials requires an ion energy of at least several keV, which increases with the desired depth of implantation. It is assumed that 2D materials should be implanted with reduced energies [2]. Regardless of whether ultra-low-energy or high-energy ions were used in the implantation process, an important aspect is the ability to assess the consequences of the process and thus change in the material properties. [3,4].

An important group of 2D materials is transition metal dichalcogenides (TMDCs) such as MoS_2, WS_2, $MoSe_2$, $MoTe_2$, WSe_2, and WTe_2 which have dominated the research interest and evolution of quasi-two-dimensional materials due to their variety of structure and application possibilities [5,6]. In this paper, we are focused on the implantation process of molybdenum disulfide 2D structure. Molybdenum disulfide (MoS_2), as the flagship representative of TMDCs, has attracted intensive attention due to its promising properties. MoS_2 has the advantages of abundant reserves, low cost, favorable biocompatibility, good mechanical properties, and high chemical stability. 2D MoS_2 has also unique optical [7-9], catalytical [10,11], and electrical [12,13] properties. MoS_2 has a stable structure consisting of hexagonal layers co-bonded via Van der Waals forces, and each layer has covalent bonds between Mo and S (S-Mo-S). This material is categorized as a semiconducting material with tunable bandgap energy from 1.2 eV for bulk MoS_2, to 1.8 eV in monolayer with various ranges of applications as a component of batteries [14], transistors [8], or optoelectronics devices [9]. What is important the value of the band gap depends on the structure of the 2D materials and it is indirect for the bulk MoS_2 whereas the monolayer counterpart is direct. The direct band gap in 2 D Transition metal dichalcogenides (TMDs) of which MoS_2 is an example depends on the localized d orbital of the Transition metal (TM) which is minimum affected by the interlayer coupling due to its location in the unit cell. While the indirect band gap in these materials depends on the

* Corresponding author.
E-mail address: Sylwia.Kozdra@imif.lukasiewicz.gov.pl (S. Kozdra).

https://doi.org/10.1016/j.apsusc.2023.157547
Received 14 March 2023; Received in revised form 9 May 2023; Accepted 15 May 2023
Available online 18 May 2023
0169-4332/© 2023 The Authors. Published by Elsevier B.V. This is an open access article under the CC BY license (http://creativecommons.org/licenses/by/4.0/).

overlap of the d orbital of TM and pz orbital of the chalcogenide atoms which strongly depends on inter-layer coupling. Thus as the number of layers is decreased the intrinsic direct band gap of the material becomes more pronounced. While the band gap broadening in a single layer is due to the quantum confinement effect of charge carriers which is common in nanosystems [15].

Changes in the structure of the MoS_2 monolayer allow to get new combinations of properties, and thus open up new application possibilities. MoS_2 defects can take the form of impurities but also intentionally created heterostructures, which are created to introduce specific elements and their properties into the structure of 2D MoS_2. Therefore, studying the properties of TMDs and their heterostructures is of great significance for further understanding their intrinsic physics and developing more practical applications. Layered 2D MoS_2 is a material that shows promising properties for use in photovoltaics and its band gap value can be estimated using the DFT technique [16]. The analysis of electrical properties in the case of materials with an ordered structure is commonly carried out for periodic models [17-19], and also for MoS_2 heterostructures with MoO_3 [20].

Heterostructures can be constructed in both vertical and horizontal directions. Vertically, by combining 2D layered compounds with other nanomaterials such as quantum dots and 1D nanowires/bands [21]. MoS_2 heterostructures find many applications, including in photovoltaics, medicine, optoelectronics, and many others [22]. MoS_2/MoO_3 is one example of a 2D-3D heterostructure [23,24]. α-MoO_3 is an n-type semiconductor with a layered crystal structure with a wide band gap of 3.2 eV [25]. Molybdenum trioxide as a transition metal oxide has high chemical and thermal stability. Due to their electrical properties, the MoO_3 oxide could be incorporated into transistors to improve the combination of conductive/insulating properties [26]. Nano-sized MoO_3 combined in heterostructures have been utilized in various applications, such as electrochromic/photochromic devices, pseudocapacitive charge storage, supercapacitors, gas sensors, lithium-ion batteries, and effective heterogeneous catalysts [27-32]. Although many attempts have been made to introduce defects into 2D materials [33-36], the mechanism of implantation is not fully understood [2]. Therefore, it is crucial to use a variety of techniques, both theoretical and instrumental analysis, to allow insight into the structure of 2D materials.

Theoretical techniques provide invaluable support in the analysis of the properties of 2D materials, including MoS_2 [37]. Structural, as well as electrical and catalytic properties, could be determined through the use of theoretical techniques including Density Functional Theory (DFT) [38-40]. The DFT technique is a suitable tool for predicting the properties of MoS2. Additional improvements, such as dispersion interactions and long-range interaction corrections [41] are increasingly taken into account. Long-range correction improved the reproducibility of van der Waals bonds, has also solved the underestimations of charge transfer excitation energies and oscillator strengths in time-dependent Kohn–Sham calculations, and has clearly improved poor optical response [42].The positive impact of using interaction correction in DFT calculations depends on the functional used (B3LYP, PBE, or M062X, and M11) but above all on the type of structure being analyzed and the atoms that make up this structure and affect van der Waals interactions. There are reports of using interaction correction for MoS2 and MoO3 structures, especially in periodic models where Van der Waals interactions play an important role [43]. Calculations for TMDCs structures based on polar functions, e.g. B3LYP, without interaction corrections, were also analyzed and their results were successfully compared to experimental results [38,44,45]. The introduction of additional details to the computational model resulted in an increase in their cost, therefore the calculations were carried out on the basis of a balance between the benefit of the most accurate results and the computational cost of the processes and their time-consuming nature.

The Raman spectroscopy technique has been popularly used to analyze the structure of 2D materials and the evolution of structural parameters in layered materials, for example, to study the quality and layer number of graphene [46,47]. In this paper, the Raman technique allowed the characterization of 2D material and confirmed its structure, as well as the presence of components of the heterostructure. However, to estimate the depth of the occurrence of intentional impurity or accidental contamination the Secondary Ion Mass spectrometry (SIMS) technique was successfully applied.

SIMS technique originated in the previous century as a surface analytical tool to characterize materials, especially their elemental composition [48]. Unlike Raman spectroscopy, SIMS technique allows to obtain a result in the form of a depth profile, which enables the localization of individual material components [49-53].In our previous work, we used the SIMS technique to precisely analyze the composition of various materials. We successfully localized various contaminants and dopants in Graphene using a dedicated measurement procedure that combines excellent detection limits (0.8–2.9 ppm) and subnanometer depth resolution [54]. Also, 2D MoS_2 was studied using the SIMS technique with sub-nanometer depth resolution [55]. The composition and quality of MoS_2 films grown on SiO_2, $Al2O_3$, and BN substrates were investigated and compared. The destructive influence of oxygen released from substrates such as SiO_2 or Al_2O_3 during the growth process of MoS_2 was demonstrated [56]. Spectacular effects of the SIMS technique were demonstrated during the tests of materials such as MAX and MAXenes. Depth profiling of single particles of MXenes and their parent MAX phases with atomic resolution using ultralow-energy secondary-ion mass spectrometry was shown [57].

In this paper, the process of O_2^+ implantation in MoS_2 layers was investigated and described. The consequences of the implantation process, as well as the range of oxidation phenomena, have been analyzed by density-functional theory (DFT) calculations. We presented the oxidation process of the MoS_2 monolayer to thoroughly understand the temperature-induced structural response and its influence on heterostructure stability. The implanted 2D material has been characterized using Raman spectroscopy and precise depth profiles obtained with the SIMS technique with the results further compared with predictions obtained from DFT.

2. Methods

The process of oxygen implantation was analyzed using DFT theory with Gaussian 16.A01 and Gaussview 6.1.1 software package [58,59] and B3LYP functional [60,61], LANL2DZ basic set [62]. Two scenarios of gradual substitution of oxygen in place of sulfur atoms have been simulated and investigated for a monolayer cluster in a zig-zag configuration with stoichiometry Mo_nS_{2n} (n = 24), and analyse the geometry of the cluster.

The periodic calculations were performed in the aim to obtain to obtain complete and most realistic information about the electrical properties of the oxygen-implanted MoS_2 layers. Periodic cells were optimized with spin-polarized DFT calculations using the Quantum Espresso 7.1 simulation package [63,64]. 1 Ultrasoft pseudopotentials were used to describe the core electrons with the generalized gradient approximation (GGA) using the PBE2 functional including the Becke–Johnson damped D3 dispersion correction as implemented in Quantum Espresso [65,66]. The Kohn–Sham one-electron wave functions were expanded by using a plane wave basis set with a kinetic energy cutoff of 450 eV and a dense 5 × 5 × 1 Monkhorst-Pack k-point mesh over Brillouin zone is used for the geometric. An energy convergence criterion of 10–6 eV and a force convergence criterion of 0.05 eV $Å^{-1}$ were used.

The unit lattice vectors and atoms of Hexagonal MoS_2 were fully optimized in the beginning. We began the geometry optimization with the experimental lattice parameter values, which were optimized to a = b = 3.19 Å, and c = 13.38 Å. We have used (0 0 2) surface of the hexagonal MoS_2 phase was simulated by a 3 × 3 × 1 supercell model. To eliminate the artificial dipole moments within the slab model, we constructed a symmetric slab of at least two layers of Mo atoms. The slab

was separated from its periodic image by 15 Å to avoid spurious interactions between the periodic slab models.

The implantation process was performed for a few-layer MoS_2 (2D Semiconductors) sample of full area coverage. 2D material in the form of five-layers molybdenum disulfide was bombarded with a beam of O_2^+ using a CAMECA IMS SC Ultra instrument with 100 EV impact energy at a 45° incident angle. Next, the samples were annealed for one hour at 500 °C in a vacuum in order to regenerate the layered structure. The changes in the MoS_2 layered structure were characterized using the SIMS technique with Cs primary ions, 100 eV impact energy, and high incident angle of 75° to ensure the atomic depth resolution. The Renishaw inVia Raman microscope using a 532 nm wavelength obtained from a Nd:YAG laser.

3. Results

The considerations started with the $Mo_{24}S_{48}$ cluster which mimics the structure of the MoS2 layer. For this cluster, single energy calculations were performed and compared for structure spins equal to 0, 1, and 2, respectively. For this purpose, the $Mo_{24}S_{48}$ structure was optimized for multiplicity equal to 1, and then the energy of a single optimized structure was calculated for multiplicity equal to 3 and 5, respectively in Table 1. The lowest energy value was obtained for the multiplicity equal to 1, which shows that the singlet corresponds to the ground state of the molecular cluster. Calculations of the remaining structures were made assuming also multiplicities equal to 1.

During the calculations of the $Mo_{24}S_{48}$ cluster, it was assumed that the charge is 0 based on the charge of sulfur (−2) and molybdenum (+4) and the number of atoms in the cluster. Although the total charge is equal to 0, for a cluster imitating the structure of the MoS2 layer, a charge of 0 was assumed in the input files during the calculations. The results of the calculations show that the charge distribution will be different in the middle of the cluster and at its edges, which shows the Mulliken charge in the cluster using Gaussian 16.A.01 software package (Fig. 1 **SM**).

The implantation process was simulated and visualized in Fig. 1. The theoretical analysis of the phenomenon of oxygen implantation requires different approaches to the problem. The theoretical analysis included 5 stages. The first referred to the material prior to oxygen implantation. The next three were related to the gradual implantation process. Due to the different final results, two paths A and B were considered. In path A it was assumed that the oxygen implantation was concentrated in a limited area and that oxygen atoms were incorporated in the immediate vicinity of one molybdenum atom. Path B assumed that implantation was a distributed process and the incorporated oxygen atoms were not directly adjacent to each other. The last step was the post-annealing step during which the MoS_2/MoO_3 heterostructure was formed. Both scenarios assumed the same stoichiometry of changes: successively three oxygen atoms were implanted, which causes a series of changes in the structure of the $Mo_{24}S_{48}$ zig-zag cluster.

Table 1
Considerations of the single energy value, taking into account the value of spin and multiplicity of the $Mo_{24}S_{48}$ cluster (B3LYP/LANL2DZ).

Spin	Multiplicity	Single energy value, kcal/mol
0	1	−1323290,674
1	3	−1322686,569
2	5	−1322676,630

With the aim to analyze the consequences of the implanted oxygen into the molybdenum disulfide, the key stages of the oxidation process were selected and analyzed in terms of geometrical and energetic factors. The theoretical analysis included 5 stages, of which the first stage relates to the material prior to oxygen implantation. The next three relate to the gradual implantation process. Due to the different consequences, two paths were considered: A and B. In the last step, the heterostructure with MoO_3 was analyzed. The stoichiometry of investigated structure was $Mo_{23}O_{45}/MoO_3$, but in the following parts of the paper, a simplified notation: MoS_2/MoO_3 will be used. Also, part of the calculation results was presented in Supplementary materials.

4. Geometry changes

The changes in the geometry of the $Mo_{24}S_{48}$ zig-zag cluster were analyzed, both globally (monolayer cluster size) and locally (change in the length of individual bonds). Each of these analyzes showed changes caused by the oxygen implantation process. At first, the thickness (a), the lengths of its sides (b, c) as well as the diagonals (d, e) were measured (Fig. 2). The dimensions were registered for each of the stages of oxygen implantation according to the scheme shown in Fig. 1 and A and B scenarios. Changes were analyzed by calculating the difference between the dimension after oxygen implantation and the initial dimension (Table 1 **SM**) and investigated in accordance with the MoS_2/MoO_3 heterostructure (Fig. 3, Fig. 2 **SM**). The implantation of one oxygen atom resulted from slight changes in the length of the analyzed dimensions, but the influence of building up the next ones was more visible. Both the length of the sides and diagonals increased, which was caused by the inclusion of oxygen with an additional free electron pair. The dimension which was least sensitive to changes in the geometry of the local layer was its thickness (a). However, the formation of the MoO_3 molecule caused a change in the trend of the local geometry of the monolayer toward the reduction of the analyzed dimensions and towards the return to their original values.

The bond length dispersion of the molybdenum disulfide sheet was considered as a measure of layer stability and was examined by analysis of the differences between the longest and the shortest bonds in the monolayer (Fig. 4, Table 2 **SM**). For the MoS_2 structure without oxygen,

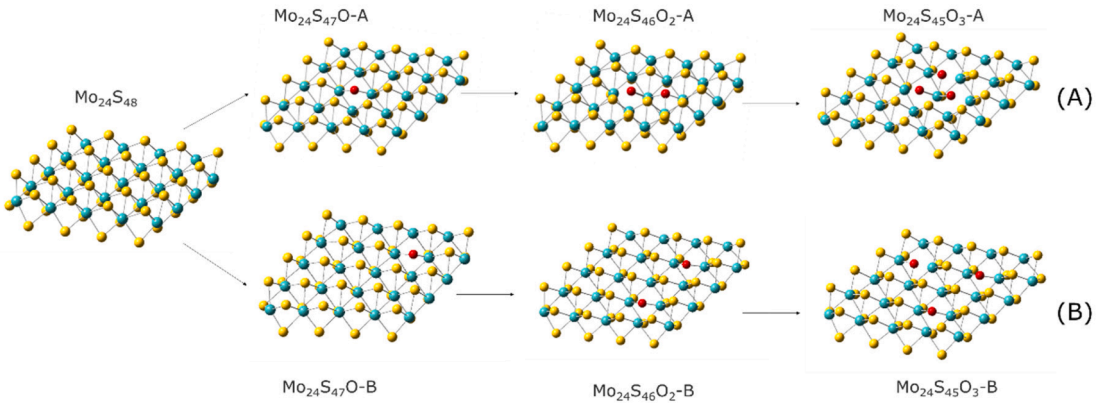

Fig. 1. Visualization of oxygen implantation process with defined structures optimized with Gaussview16.A.01 software package (B3LYP/LANL2DZ).

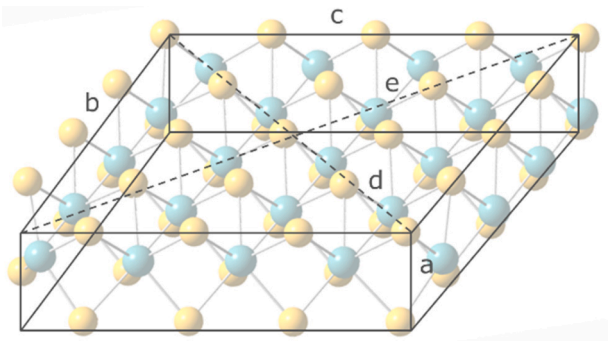

Fig. 2. Visualization of $Mo_{24}S_{48}$ cluster with the marked analyzed dimensions: thickness (a), the lengths of its sides (b, c) as well as the diagonals (d, e).

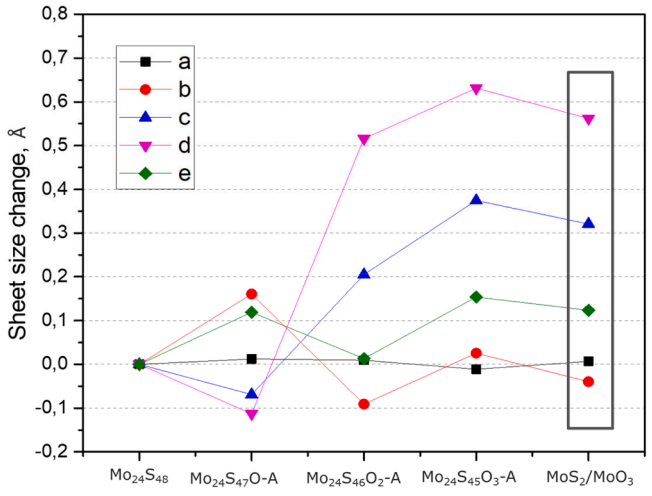

Fig. 3. Differences in values of dimensions of $Mo_{24}S_{48}$ zig-zag cluster, for structures included in investigated oxygen implantation process according to scenario A. Designations from "a" to "e", refer to the marked analyzed dimensions of the cluster structure shown in Fig. 2.

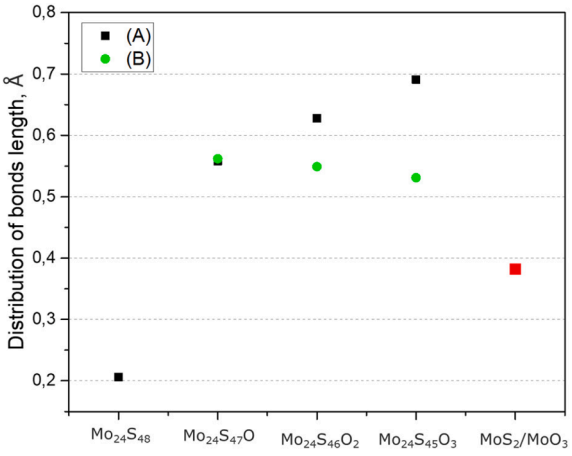

Fig. 4. The values of differences between the longest and shortest bond in the $Mo_{24}S_{48}$ zig-zag cluster as well as structures included in investigated implementation process scenarios A and B.

the difference was very small (0.206 Å) which proved the good stability of its structure. The appearance of very long or very short bonds indicates a disturbance of the existing balance and loss of stability. The bond length dispersion increased with the oxygen implantation process. The greatest changes took place near the incorporated oxygen atoms (Fig. 3 **SM**). Chemical bonds that were formed with the participation of oxygen were shortened, which could be explained by the high electronegativity of oxygen. The bonds change their character from covalent to ionic. We could observe two different trends of change for scenarios A and B. The concentrated implantation of oxygen atoms (A) gradually increased the dispersion of bond lengths, while the diffuse implantation (B) kept the dispersion at a similar level, and even decreased its value, regardless of the number of incorporated oxygen atoms. Importantly, the formation of the heterostructure resulted in a significant decrease in the dispersion of bond lengths, which could be equated with the disappearance of structural stresses. The reduction of the differences in bond length indicated greater stability of the heterostructure compared to the state in which there were bonds between MoO_3 and adjacent MoS_2 atoms.

5. MoS_2/MoO_3 stability

To clarify the stabilization of the MoO_3 in the MoS_2 structure the bonds breaking process was optimized (Fig. 5). It could be clearly seen that two stabilizing chemical bonds marked by atom numbers: Mo30-S63 and Mo35-O47 were replaced by five chemical interactions marked as dashed bonds: Mo30-S63, Mo30-S62, Mo30-S58, O42-Mo26 and O44-Mo25.

The analysis of energetic factors was performed. The visualization of total electron density mapped with electrostatic potential scale values was shown (Fig. 6 **and** Fig. 4 **SM**). The red color marked the regions rich in the electrons, which could be a donor and the blue regions marked the acceptor regions, poor in electrons. The distribution of electrons was symmetrical for each of the analyzed structures. One side of the zig-zag cluster was the donor area while the other side was the acceptor area, which indicated the possibility of undisturbed transport of electrons in the MoS_2 structure, and thus good conductive properties of the material. The oxygen incorporation regions were visible as the red, electron-rich areas, due to their electron structure. The distribution of the donor–acceptor regions showed no significant changes in location. That indicated the undisturbed charge transport within a structure, even in a heterostructure MoS_2/MoO_3.

6. HOMO & LUMO energy levels

In this work, we demonstrated the in-situ oxygen implantation of monolayer MoS_2 by introducing oxygen gas in the growth environment, we can achieve uniform oxygen doping in monolayer MoS_2 with tunable dopant concentrations, i.e., $MoS_{2-x}O_x$, without changing the lattice order. We also show the creation of in-plane heterostructures of $MoS_{2-x}O_x$ with different doping levels by tuning the oxygen gas partial pressure during the growth process. Apart from the cluster model DFT calculation further to understand the atomic and electronic properties of the pristine MoS_2 and as well as the $MoS_{2-x}O_x$ materials, we have performed preliminary periodic DFT calculations. More importantly, we found that the bandgap of monolayer $MoS_{2-x}O_x$ ca be tuned by the oxygen doping levels. The calculated band gap of pristine MoS_2 is ~1.18 eV and the band gap reduce with the implementation of oxygen into the MoS_2 surface. It has been found that with the incorporation of one, two and three oxygen the respective band gaps are 1.13 eV, 1.11 eV and 1.05 eV (Fig. 7). The values of the energy gap and its changes after the implantation of oxygen atoms indicate electronic properties that may enable the use of this type of material in high performance and low power consumption electronics.

Then, we further carried out geometrical features of these monolayer $MoS_{2-x}O_x$ materials from the periodic DFT optimized geometry (Fig. 8) and subsequent phonon calculation (vibrational analysis). Apart from the peaks present in the MoS2 intrinsic monolayer, a series of new vibrational modes appear in the $MoS_{2-x}O_x$ moiety. The new peaks at 302 cm^{-1}, 347 cm^{-1}, and 449 cm^{-1}, corresponding to the vibrational modes of Mo-O bonds, confirm the oxygen doping in monolayer MoS_2. The

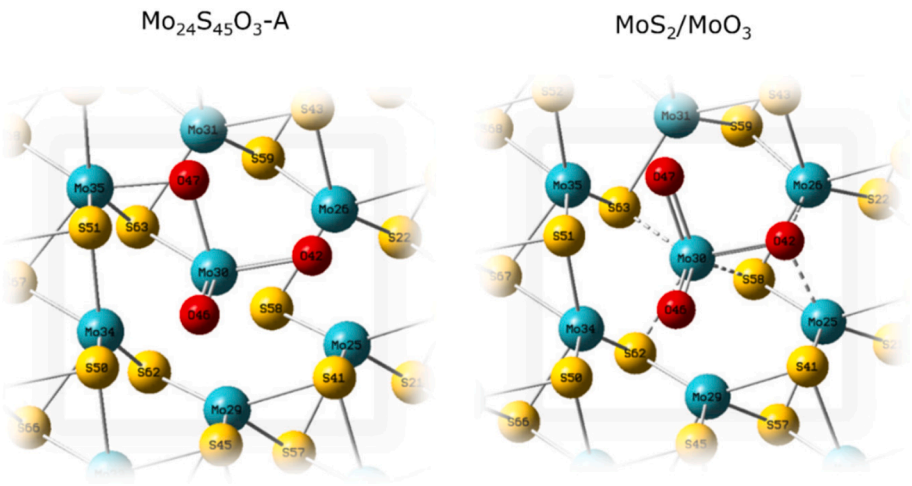

Fig. 5. Chemical bonds and interactions showed for structure $Mo_{24}S_{45}O_3$-A and heterostructure MoS_2/MoO_3.

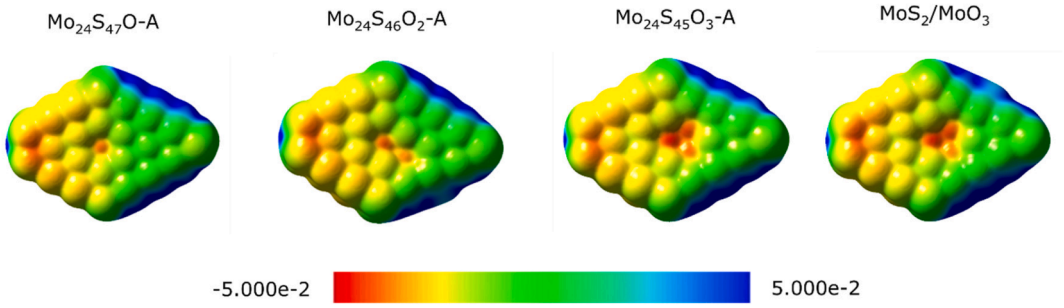

Fig. 6. Total electron density mapped with electrostatic potential scale values – visualization of the oxygen implantation process.

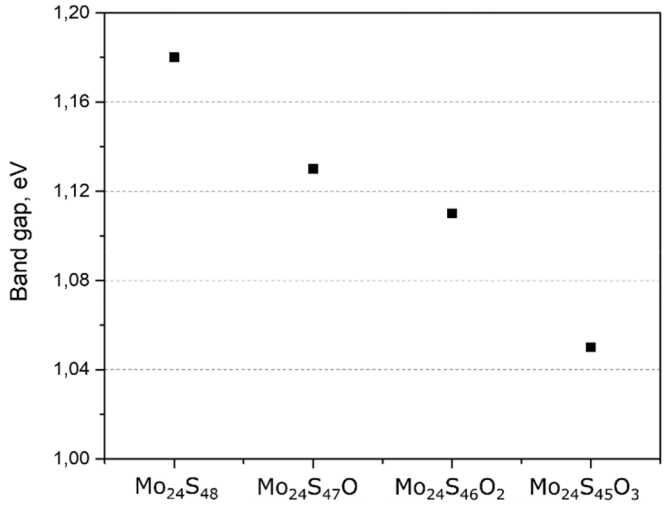

Fig. 7. Periodic DFT calculated band gap for the pristine and oxygen-dopped MoS_2 moieties.

calculated Mo-O bond length was found to be 2.31 Å which is slightly shorter than the Mo-S bond length (2.42 Å) in the pristine MoS_2 material.

Analysis of the geometry of the MoS_2 structure implemented with oxygen is consistent with the results obtained using both Gaussian and Quantum Espresso software. An example is the observation of shorter bonds between Mo-O compared to Mo-S. Significant differences were observed after comparing the electronic properties. It was considered that the value of the energy band gap for the cluster model 0,65 eV in comparison to the periodic model: 1.18–1.05 eV were closer to the bandgap values obtained experimentally 1.2–1.8 eV [14]. The analysis of HOMO and LUMO energy levels for the $Mo_{24}S_{48}$ cluster is subject to the risk of error in calculations due to the limited size of the cluster, which mimics the MoS_2 layer.

Despite this, for comparative purposes, an analysis of the energy gap of the cluster was performed using the Gaussian 16.A.01 software package, and the results are presented in SM. The position of the HOMO and LUMO orbitals visualized with Gaussview software was shown in Figs. 5 and 6 **SM**. A comparison of bandgap values shows in Fig. 7 **SM**.

7. SIMS & Raman results

Experimental methods were used to verify the possibility of the formation of a stable heterostructure. A sample of the 2D material consisting of five-layer MoS_2 was implanted with oxygen and the structure of the material was examined before and after exposing the sample to oxygen, also after annealing the sample. The effects of oxygen implantation on 2D MoS_2 and changes in the sample's structure at each stage of the experiment were studied using Raman spectroscopy and SIMS techniques.

Raman spectroscopy technique provided information about chemical state and the type of interactions inside the material. The Raman spectra for the sample before implantation, after implantation, as well as after annealing were presented and compared (Fig. 9). Before bombardment two dominating peaks were observed at 382,3 cm^{-1} and 407,6 cm^{-1} that could be assigned with the in-plane vibration of two S atoms with respect to the Mo atom, and out-of-plane vibration of S atoms in opposite directions (Table 2), [67,68]. Raman spectrum measured after the bombardment of MoS_2, with O_2^+ ions, reveals a significant reduction of the intensity of the noted peaks that confirmed the deterioration of MoS_2

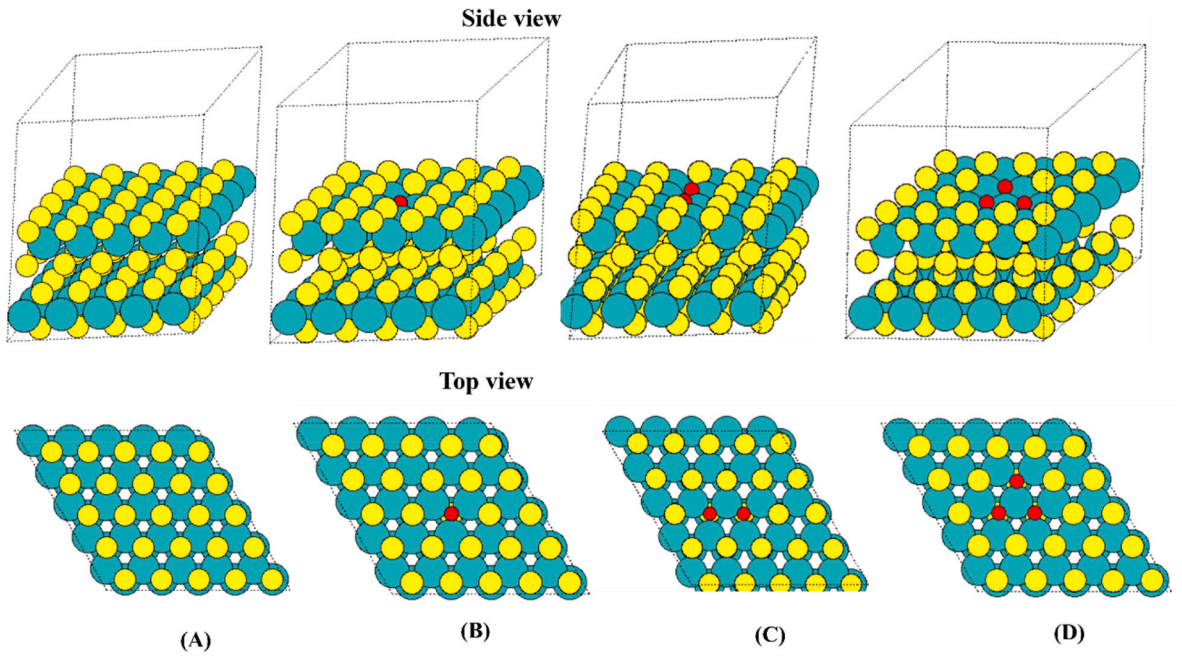

Fig. 8. The DFT optimized structure of the supercell used for the calculation. We show the side view and top view of 3 × 3 (A) pristine monolayer MoS_2. S is substituted by (B) a single, (C) double and (D) triple oxygen implantation. teal spheres indicate Mo atoms; yellow spheres indicate S; red spheres indicate O atoms. (For interpretation of the references to color in this figure legend, the reader is referred to the web version of this article.)

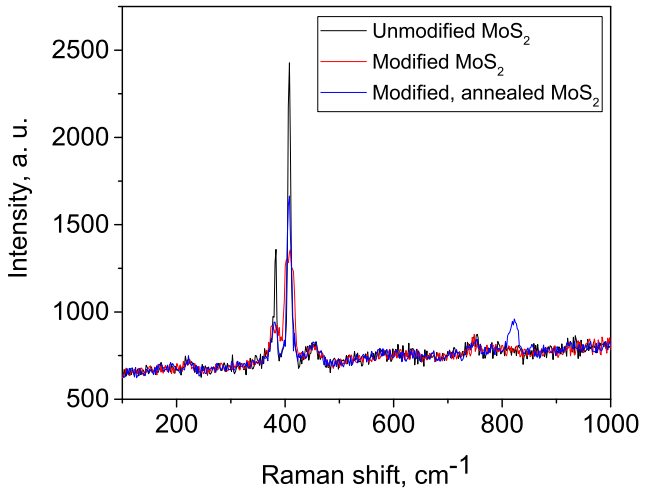

Fig. 9. Raman spectra obtained for the MoS_2 sample with marked signals: unmodified (black), implanted with oxygen ions (red), and after annealing (blue). (For interpretation of the references to color in this figure legend, the reader is referred to the web version of this article.)

Table 2
Interpretation of the Raman spectra for MoS_2 samples.

Signal position, cm^{-1}	Interpretation
382,3 407,6	MoS_2: in-plane vibration of two S atoms with respect to the Mo atom, and out-of-plane vibration of S atoms in opposite directions
821,1	α-MoO_3: doubly coordinated oxygen (Mo_2-O) stretching mode, which results from corner-sharing oxygen atoms common to two octahedral

2D structure. After annealing, the intensity of the MoS_2 peaks increased, suggesting an improvement in the quality of the ordering of the structure which could result from partial healing of the defects formed after oxygen bombardment due to temperature treatment. Moreover, after annealing a new, previously unobserved maximum appears around 821 cm^{-1} indicating the presence of α-MoO_3 [69-71].

The analysis using the SIMS technique provided precise information on the location of sulfur, molybdenum, and oxygen in the tested sample. SIMS measurements with sub-nanometer resolution confirmed the existence of five MoS_2 layers in the analyzed sample (Fig. 10). Distinct maxima for molybdenum and sulfur of fully distinguished five MoS_2 layers were observed. The shape of the depth profile, and more precisely the number of counts for oxygen in the first three MoS_2 layers, showed that oxygen occupies sulfur vacancies, bonding with molybdenum.

Significant structure changes were noted after oxygen implantation. The 2D structure of the first three MoS_2 layers was vitally disturbed, the numbers of sulfur and molybdenum counts change, and the amount of detected oxygen increased forming a typical implantation profile. The effect of destroying the 2D structure could be explained by the bombardment of beam ions O_2^+ to the material, which, by building into the 2D structure, caused a mixing effect. The healing of the structure could be observed after annealing at a temperature of 500 °C for 1 h. Despite the reconstruction of the MoS_2 structure and the restoration of the characteristics of the 2D material, oxygen remained built into the structure. It can be noted that all Mo peaks have been recreated and they look practically identical to those registered for the unmodified structure. However, the intensity of sulfur peaks in the first three layers has slightly decreased (by 5–20%). A comparison of the signal intensity of sulfur and oxygen before and after annealing on a linear scale was shown in the SM (Fig. 7 **SM**). The oxygen signal no longer preserves the shape of an implantation profile and a clear agglomeration can be seen at positions where sulfur depletion has been observed. It strongly indicates that oxygen occupies sulfur vacancies, bonding with molybdenum.

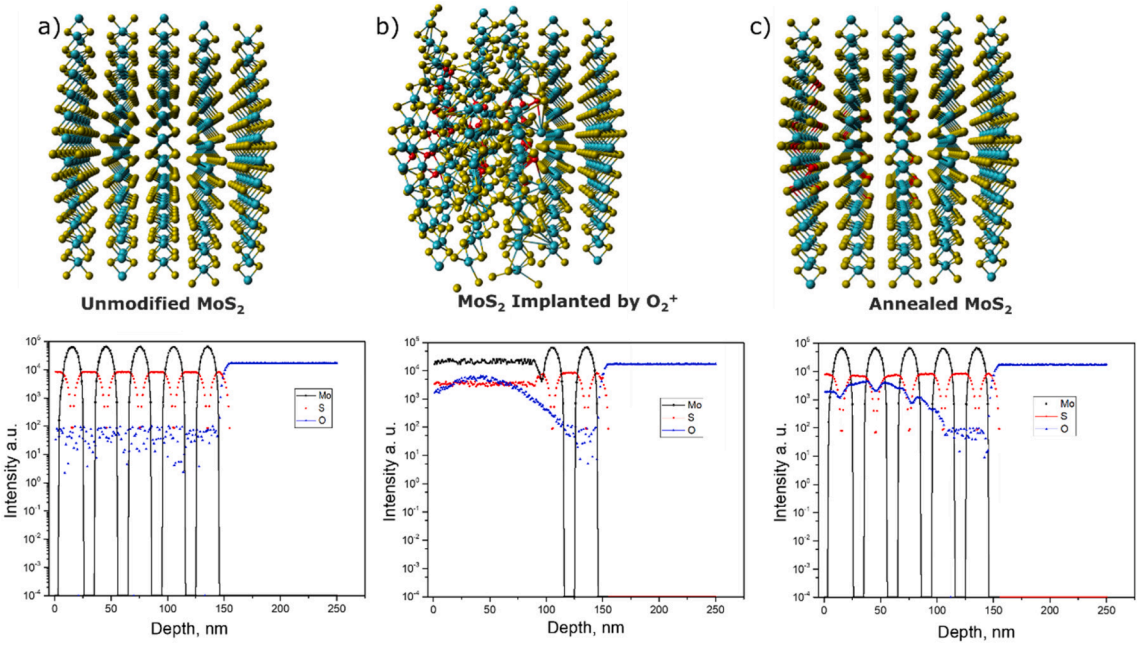

Fig. 10. Depth profiles measured using Secondary Ion Mass Spectrometry technique for a) unmodified, b) Implanted using O_2^+, and c) annealed MoS_2 sample.

8. Discussion

Structural changes and, consequently, changes in properties occur under the influence of oxygen implantation, regardless of the assumed scenario A or B. It could be clearly stated that the process of random incorporation of oxygen atoms has a different effect compared to implantation, which leads to the formation of a MoS_2/MoO_3 heterostructure. The formation of MoO_3 particles in the MoS_2 structure allowed the restoration of the geometrical and energetic stability as has been shown by DFT calculations. The use of two models made it possible to confirm the changes in the geometry of the model during oxygen implantation and the changes in energy properties expressed by the value of the energy band gap. While the changes in bond lengths are cumulative both for the results presented for the cluster and periodic model, the changes in the energy band gap value differ depending on the model used. Comparison with experimental data clearly shows that the model closer to realism is the periodic model. At the same time, the results of experimental studies showed that the oxygen implantation of MoS_2 layers and subsequent annealing leads to the formation of MoO_3. It was demonstrated that the applied implantation technique allowed to successfully produce a MoS_2/MoO_3 conductive/insulating heterostructure with changed properties.

9. Conclusions

The implantation of oxygen and replacing the sulfur atom caused significant changes in the structure of the 2D material. Significant disorganization and a change in the length of the chemical bonds were shown, as well as changes to the global geometry of the MoS_2 cluster. The area and depth of the occurring changes were precisely determined using the SIMS technique. During the DFT calculations, a scenario was proposed in which breaking chemical bonds leads to the formation of the MoO_3 molecule in the MoS_2 structure. 2D material regains its orderly character as demonstrated using experimental and theoretical techniques. We showed that by implanting, it is possible to selectively oxidize MoS_2 and form MoO_3 and thus create a semiconductive/insulating heterostructure. These superior electrical properties of oxygen implemented MoS_2 monolayer suggest their potentials for high performance and low power consumption electronics.

It is found that 2D materials could be successfully investigated using SIMS, Raman, and DFT techniques. Quantum chemical techniques made it possible to predict the oxidation of MoS_2 towards MoO_3, while the use of instrumental techniques precisely determined the area of occurrence of the most significant changes in the structure.

Data availability:

All relevant data are available from the authors on reasonable request, and/or are included within the Article and the Supplementary Information.

CRediT authorship contribution statement

This research was performed at the Łukasiewicz Research Network - Institute of Microelectronics and Photonics. Conceptualization, DFT investigation, calculations, analysis, (Sylwia Kozdra), Secondary Ion Mass Spectrometry & Raman studies, (Paweł Piotr Michałowski), Raman Spectroscopy analysis (Adrianna Wójcik), results visualization (Sylwia Kozdra), periodic model calculation and results investigation (Tamal Das).

Declaration of Competing Interest

The authors declare that they have no known competing financial interests or personal relationships that could have appeared to influence the work reported in this paper.

Data availability

Data will be made available on request.

Acknowledgments

This work was supported by the National Science Centre within the SONATA14 (grant no. 2018/31/D/ST5/00399 to P.P.M.). This work was also supported by the Interdisciplinary Centre for Mathematical and

Computational Modelling in Warsaw for providing computer facilities for the possibility of performing quantum-mechanical calculations under grant No.G89-1270 (to S.K.). S.K and T.D. acknowledge the support from the Research Council of Norway through the Centre of Excellence (No. 262695). T. D. thanks the Norwegian Metacenter for Computational Science (NOTUR) for computational resources (No. nn4654k).

Appendix A. Supplementary data

Supplementary data to this article can be found online at https://doi.org/10.1016/j.apsusc.2023.157547.

References

[1] S. Sovizi, R. Szoszkiewicz, Single atom doping in 2D layered MoS_2 from a periodic table perspective, Surf. Sci. Rep. 77 (2022) 3, https://doi.org/10.1016/j.surfrep.2022.100567.
[2] M.N. Bui, S. Rost, M. Auge, J.-S. Tu, L. Zhou, I. Aguilera, S. Blügel, M. Ghorbani-Asl, A.V. Krasheninnikov, A. Hashemi, H.-P. Komsa, L. Jin, L. Kibkalo, E. N. O'Connell, Q.M. Ramasse, U. Bangert, H.C. Hofsäss, D. Grützmacher, B. E. Kardynal, Low-energy Se ion implantation in MoS_2 monolayers, npj 2D Mater. Appl. 6 (2022) 42, https://doi.org/10.1038/s41699-022-00318-4.
[3] Y.-C. Lin, C. Liu, Y. Yu, E. Zarkadoula, M. Yoon, A.A. Puretzky, L. Liang, X. Kong, Y. Gu, A. Strasser, H.M. Meyer III, M. Lorenz, M.F. Chisholm, I.N. Ivanov, C. M. Rouleau, G. Duscher, K. Xiao, D.B. Geohegan, Low energy implantation into transition-metal dichalcogenide monolayers to form Janus structures, ACS Nano 14 (4) (2020) 3896–3906, https://doi.org/10.1021/acsnano.9b10196.
[4] U. Bangert, A. Stewart, E. O'Connell, E. Courtney, Q. Ramasse, D. Kepaptsoglou, H. Hofsäss, J. Amani, J.-S. Tu, B. Kardynal, Ion-beam modification of 2-D materials - single implant atom analysis via annular dark-field electron microscopy, Ultramicroscopy 176 (2017) 31–36, https://doi.org/10.1016/J.ULTRAMIC.2016.12.011.
[5] A. Arafat, M.S. Islam, N. Ferdous, A.S.M.J. Islam, M.M.H. Sarkar, C. Stampfl, J. Park, Atomistic reaction mechanism of CVD grown MoS_2 through MoO_3 and H2S precursors, Sci. Rep. 12 (2022) 16085, https://doi.org/10.1038/s41598-022-20531-x.
[6] S.A. Han, R. Bhatia, S.-W. Kim, Synthesis, properties and potential applications of two-dimensional transition metal dichalcogenides, Nano Converg. 2 (2015) 17, https://doi.org/10.1186/s40580-015-0048-4.
[7] T. Hu, R. Zhang, J.-P. Li, J.-Y. Cao, F. Qiu, Photodetectors based on two-dimensional MoS_2 and its assembled heterostructures, Chip 1 (2022) 3, https://doi.org/10.1016/j.chip.2022.100017.
[8] A. Molina-Sánchez, K. Hummer, L. Wirtz, Vibrational and optical properties of MoS_2: from monolayer to bulk, Surf. Sci. Rep. 70 (4) (2015) 554–586, https://doi.org/10.1016/J.SURFREP.2015.10.001.
[9] V. Hasija, P. Raizada, V.K. Thakur, A.A.P. Khan, A.M. Asiri, P. Singh, An overview of strategies for enhancement in photocatalytic oxidative ability of MoS_2 for water purification, Environ. Chem. Eng. 8 (5) (2020), 104307, https://doi.org/10.1016/J.JECE.2020.104307.
[10] J. Tang, J. Huang, D. Ding, S. Zhang, X. Deng, Research progress of 1T-MoS_2 in electrocatalytic hydrogen evolution, Int. J. Hydrog. Energy. 47 (94) (2022) 39771–39795, https://doi.org/10.1016/J.IJHYDENE.2022.09.162.
[11] M.-H. Wu, L. Li, N. Liu, D.J. Wang, Y. Ch Xue, L. Tang, Molybdenum disulfide (MoS_2) as a co-catalyst for photocatalytic degradation of organic contaminants: a review, Process Saf. Environ. Prot. 118 (2018) 40–58, https://doi.org/10.1016/J.PSEP.2018.06.025.
[12] E. Ghaleghafi, M.B. Rahmani, M. b., Exploring different routes for the synthesis of 2D MoS_2/1D PANI nanocomposites and investigating their electrical properties, Physica E Low Dimens. Syst. Nanostruct. 138 (2022), 115128, https://doi.org/10.1016/J.PHYSE.2021.115128.
[13] L. Lei, D. Huang, G. Zeng, M. Cheng, D. Jiang, C.h. Zhou, S.h. Chen, W. Wang, A fantastic two-dimensional MoS_2 material based on the inert basal planes activation: electronic structure, synthesis strategies, catalytic active sites, catalytic and electronics properties, Coord. Chem. Rev. 399 (2019), 213020, https://doi.org/10.1016/J.CCR.2019.213020.
[14] E. Cha, M.D. Patel, J. Park, J. Hwang, V. Prasad, K. Cho, W. Choi, 2D MoS_2 as an efficient protective layer for lithium metal anodes in high-performance Li–S batteries, Nat. Nanotech. 13 (2018) 337–344, https://doi.org/10.1038/s41565-018-0061-y.
[15] J.K. Ellis, M.J. Lucero, G.E. Scuseria, The indirect to direct band gap transition in multilayered MoS_2 as predicted by screened hybrid density functional theory, Appl. Phys. Lett. 99 (2011), 261908.
[16] W. Dhiman, N. Kondal, MoS_2–ZnO nanocomposites for photocatalytic energy conversion and solar applications, Physica B Condens. 628 (2022), 413569, https://doi.org/10.1016/j.physb.2021.413569.
[17] S.h. Deng, L. Li, M. Li, Stability of direct band gap under mechanical strains for monolayer MoS_2, $MoSe_2$, WS_2 and WSe_2, Physica E Low Dimens. 101 (2018) 44–49, https://doi.org/10.1016/j.physe.2018.03.016.
[18] V.A. Khalas, W.B. Parmar, A.M. Vora, A density functional theory based study of transition metal dichalcogenide - MoS_2, Mater. Today: Proc. 67 (1) (2022) 165–169, https://doi.org/10.1016/j.matpr.2022.06.012.
[19] A. Bano, A.K. Gaur, Electronic and thermal properties of monolayer MoS_2: a first-principles study, Mater. Today: Proc 47 (18) (2021) 6464–6468, https://doi.org/10.1016/j.matpr.2021.08.183.
[20] S. Feng, C. Liu, Q. Zhu, X. Su, W. Qian, Y. Sun, C.h. Wang, B. Li, M. Chen, L. Chen, W. Chen, L. Zhang, F. Wang, W. Ren, L. Yin, X. Wang, H.-M. Cheng, D.-M. Sun, An ultrasensitive molybdenum-based double-heterojunction phototransistor, Nat. Commun. 12 (2021) 4094, https://doi.org/10.1038/s41467-021-24397-x.
[21] W. Li, Z. Yang, M. Sun, J. Dong, Interlayer interactions in transition metal dichalcogenides heterostructures, Rev. 9 (2022), 100077, https://doi.org/10.1016/J.REVIP.2022.100077.
[22] X. Li, H. Zhu, Two-dimensional MoS_2: properties, preparation, and applications, J. Materiomics. 1 (1) (2015) 33–44, https://doi.org/10.1016/J.JMAT.2015.03.003.
[23] P. Qin, G. Fang, W. Ke, F. Cheng, Q. Zheng, J. Wan, H. Lei, X. Zhao, In situ growth of double-layer MoO3/MoS_2 film from MoS_2 for hole-transport layers in organic solar cell, J. Mater. Chem. A 2 (2014) 2742–2756, https://doi.org/10.1039/C3TA13579A.
[24] S. Singh, J. Deb, U. Sarkar, S. Sharma, MoS_2/MoO_3 nanocomposite for selective NH3 detection in a humid environment, ACS Sustain. Chem. Eng. 9 (21) (2021) 7328–7340, https://doi.org/10.1021/acssuschemeng.1c01527.
[25] S. Bandaru, G. Saranya, N.J. English, C. Yam, M. Chen, Tweaking the electronic and optical properties of α-MoO3 by sulphur and selenium doping – a density functional theory study, Sci. Rep. 8 (2018) 10144, https://doi.org/10.1038/s41598-018-28522-7.
[26] Q. Tang, L. Wang, K. Zhu, Z. Shan, X. Qin, Synthesis and electrochemical properties of H-MoO3/graphene composite, Mater. Lett. 100 (2013) 127–129, https://doi.org/10.1016/J.MATLET.2013.03.005.
[27] T. Ghrib, A.L. Al-Otaibi, M. Alqahtani, N.A. Altamimi, A. Bardaoui, S. Brini, Structural, optical and electrical properties of the Zn doped MoO3 deposited on porous silicon, Sens. Actuator A Phys. 297 (2019), 111537, https://doi.org/10.1016/J.SNA.2019.111537.
[28] T. Brezesinski, J. Wang, S.H. Tolbert, B. Dunn, Ordered mesoporous α-MoO3 with iso-oriented nanocrystalline walls for thin-film pseudocapacitors, Nat. Mater. 9 (2010) 146–151, https://doi.org/10.1038/nmat2612.
[29] S.S. Sunu, E. Prabhu, V. Jayaraman, K.I. Gnanasekar, T.K. Seshagiri, T. Gnanasekaran, Electrical conductivity and gas sensing properties of MoO3, Sens. Actuators B Chem. 101 (1–2) (2004) 161–174, https://doi.org/10.1016/J.SNB.2004.02.048.
[30] O. Lupan, V. Cretu, M. Deng, D. Gedamu, I. Paulowicz, S. Kaps, Y.K. Mishra, O. Polonskyi, C.h. Zamponi, L. Kienle, V. Trofim, I. Tiginyanu, R. Adelung, Versatile growth of freestanding orthorhombic α-molybdenum trioxide nano- and microstructures by rapid thermal processing for gas nanosensors, J. Phys. Chem. C 118 (27) (2014) 15068–15078, https://doi.org/10.1021/jp5038415.
[31] S.-H. Lee, Y.-H. Kim, R. Deshpande, P.A. Parilla, E. Whitney, D.T. Gillaspie, K. M. Jones, A.H. Mahan, S.h. Zhang, A.C. Dillon, Reversible lithium-ion insertion in molybdenum oxide nanoparticles, Adv. Mater. 20 (2008) 3627–3632, https://doi.org/10.1002/adma.200800999.
[32] A. Michailovski, J.-D. Grunwaldt, A. Baiker, R. Kiebach, W. Bensch, G.R. Patzke, Studying the solvothermal formation of MoO3 fibers by complementary in situ EXAFS/ EDXRD techniques, Angew. Chem. Int. Ed. 44 (2005) 5643–5647, https://doi.org/10.1002/anie.200500514.
[33] U. Bangert, W. Pierce, D.M. Kepaptsoglou, Q. Ramasse, R. Zan, M.H. Gass, J.A. Van den Berg, C.B. Boothroyd, J. Amani, H. Hofsäss, Ion implantation of graphene—toward IC compatible technologies, Nano Lett. 13 (10) (2013) 4902–4907, https://doi.org/10.1021/nl402812y.
[34] S. Mignuzzi, A.J. Pollard, N. Bonini, B. Brennan, I.S. Gilmore, M.A. Pimenta, D. Richards, D. Roy, Effect of disorder on Raman scattering of single-layer MoS_2, Phys. Rev. B 91 (2015), 195411, https://doi.org/10.1103/PhysRevB.91.195411.
[35] L. Madauß, O. Ochedowski, H. Lebius, B. Ban-d'Etat, C.H Naylor, A.T.Ch. Johnson, J. Kotakoski, M. Schleberger, Defect engineering of single- and few-layer MoS_2 by swift heavy ion irradiation. 2D Mater. 4(1) (2016) 015034. 10.1088/2053-1583/4/1/015034.
[36] A. Nipane, D. Karmakar, N. Kaushik, S. Karande, S. Lodha, Few-layer MoS_2 p-type devices enabled by selective doping using low energy phosphorus implantation, ACS Nano 10 (2) (2016) 2128–2137, https://doi.org/10.1021/acsnano.5b06529.
[37] X. Lin, W. Li, Y. Dong, C.h. Wang, Q. Chen, H. Zhang, Two-dimensional metallic MoS_2: a DFT study, Comput. Mater. Sci. 124 (2016) 49–53, https://doi.org/10.1016/J.COMMATSCI.2016.07.020.
[38] M. Javaid, D.W. Drumm, S.P. Russo, A.D. Greentree, A study of size-dependent properties of MoS_2 monolayer nanoflakes using density-functional theory, Sci. Rep. 7 (2017) 9775, https://doi.org/10.1038/s41598-017-09305-y.
[39] P. Chandra, A. Mohammad, B. Tripathi, T. Yoon, Recent advancements in molybdenum disulfide (MoS_2) and its functional nanostructures for photocatalytic and non-photocatalytic organic transformations, FlatChem 34 (2022), 100395, https://doi.org/10.1016/J.FLATC.2022.100395.
[40] B. Gao, J.-R. Zhang, L. Chen, J. Guo, S.h. Shen, A.u. Ch-T, Sh-F. Yin, M-Q. Cai,, Density functional theory calculation on two-dimensional MoS_2/BiOX (X = Cl, Br, I) van der Waals heterostructures for photocatalytic action, Appl. Surf. Sci. 492 (2019) 157–165, https://doi.org/10.1016/J.APSUSC.2019.06.201.
[41] S. Grimme, A. Hansen, J.G. Brandenburg, C.h. Bannwarth, Dispersion-corrected mean-field electronic structure methods, Chem. Rev. 116 (9) (2016) 5105–5154, https://doi.org/10.1021/acs.chemrev.5b00533.
[42] T. Tsuneda, K. Hirao, Long-range correction for density functional theory, Wiley Interdiscip. Rev. Comput. Mol. Sci. 4 (4) (2014) 375–390, https://doi.org/10.1002/wcms.1178.

[43] H. Peelaers, C.G. Van de Walle, First-principles study of van der Waals interactions in MoS_2 and MoO_3, J. Phys. Condens. J. Phys.: Condens. Matter 26 (2014), 305502, https://doi.org/10.1088/0953-8984/26/30/305502.
[44] Z. Hashemi, S. Rafiezadeh, R. Hafizi, S.J. Hashemifar, H. Akbarzadeh, First-principles study of MoS_2 and MoSe2 nanoclusters in the framework of evolutionary algorithm and density functional theory, Chem. Phys. Lett. 698 (2018) 41–50, https://doi.org/10.1016/j.cplett.2018.03.008.
[45] J. Saju, T. Simil, M. Jainy, S.K. Anusha, T.J. Sruthi, T. Sabu, K. Nandakumar, Theoretical study on tuning band gap and electronic properties of atomically thin nanostructured MoS_2/metal cluster heterostructures, ACS Omega 6 (10) (2021) 6623–6628, https://doi.org/10.1021/acsomega.0c05274.
[46] M.A. Pimenta, E. del Corro, B.R. Carvalho, C. Fantini, L.M. Malard, Comparative study of Raman spectroscopy in graphene and MoS_2-type transition metal dichalcogenides, Acc. Chem. Res. 48 (1) (2014) 41–47, https://doi.org/10.1021/ar500280m.
[47] B.C. Windom, W.G. Sawyer, D.W. Hahn, A Raman spectroscopic study of MoS_2 and MoO3: applications to tribological systems, Tribol. Lett. 42 (2011) 301–310, https://doi.org/10.1007/s11249-011-9774-x.
[48] E.G. Seebauer, D.E. Barlaz, SIMS for analysis of nanostructures, Curr. Opin. Chem. Eng. 12 (2016) 8–13, https://doi.org/10.1016/J.COCHE.2016.01.007.
[49] D.S. Francischini, M.A.Z. Arruda, When a picture is worth a thousand words: molecular and elemental imaging applied to environmental analysis – a review, Microchem. J. 169 (2021), 106526, https://doi.org/10.1016/J.MICROC.2021.106526.
[50] H. Xiong, W. Mao, R. Wang, S.h. Liu, N. Zhang, L. Song, D. Yang, X. Pi, Characterizations on the doping of single-crystal silicon carbide, Mater. Today Phys. 29 (2022), 100906, https://doi.org/10.1016/J.MTPHYS.2022.100906.
[51] J.S. Fletcher, J.C. Vickerman, N. Winograd, Label free biochemical 2D and 3D imaging using secondary ion mass spectrometry, Curr. Opin. Chem. Biol. 15 (5) (2011) 733–740, https://doi.org/10.1016/J.CBPA.2011.05.016.
[52] M. Collin, S. Gin, P. Jollivet, L. Dupuy, V. Dauvois, L. Duffours, ToF-SIMS depth profiling of altered glass, NPJ Mater. Degrad. 3 (2019) 14, https://doi.org/10.1038/s41529-019-0076-3.
[53] F. Adams, L. van Vaeck, R. Barrett, Advanced analytical techniques: platform for nano materials science, Spectrochim. Acta B: At. Spectrosc. 60 (1) (2005) 13–26, https://doi.org/10.1016/J.SAB.2004.10.003.
[54] P.P. Michałowski, S. Kozdra, I. Pasternak, J. Sitek, A. Wójcik, W. Strupiński, Precise localization of contaminants in graphene with secondary ion mass spectrometry, Measurement 187 (2022), 110308, https://doi.org/10.1016/J.MEASUREMENT.2021.110308.
[55] P.P. Michałowski, P. Knyps, P. Ciepielewski, P. Caban, E. Dumieszewska, J. Baranowska, Destructive role of oxygen in growth of molybdenum disulfide determined by secondary ion mass spectrometry, Phys. Chem. Chem. Phys. 21 (2019) 8837, https://doi.org/10.1039/C9CP00613C.
[56] P.P. Michałowski, P. Knyps, P. Ciepelewski, P.A. Caban, E. Duieszewska, G. Kowalski, M. Tokarczyk, J.M. Baranowski, Growth of highly oriented MoS_2 via an intercalation process in the graphene/SiC(0001) system, Phys. Chem. Chem. Phys. 21 (2019) 20641, https://doi.org/10.1039/C9CP03846A.
[57] P.P. Michałowski, M. Anayee, T.S. Mathis, S. Kozdra, A. Wójcik, K. Hantanasirisakul, I. Jóźwik, A. Piątkowska, M. Możdżonek, A. Malinowska, R. Diduszko, E. Wierzbicka, Y. Gogotsi, Oxycarbide MXenes and MAX phases identification using monoatomic layer-by-layer analysis with ultralow-energy secondary-ion mass spectrometry, Nat. Nanotechnol. 17 (2022) 1192–1197, https://doi.org/10.1038/s41565-022-01214-0.
[58] M.J. Frisch, G.W. Trucks, H.B. Schlegel, G.E. Scuseria, M.A. Robb, J.R. Cheeseman, G. Scalmani, V. Barone, G.A. Petersson, H. Nakatsuji, X. Li, M. Caricato, A.V. Marenich, J. Bloino, B.G. Janesko, R. Gomperts, B. Mennucci, H.P. Hratchian, J.V. Ortiz, A.F. Izmaylov, J.L. Sonnenberg, D. Williams-Young, F. Ding, F. Lipparini, F. Egidi, J. Goings, B. Peng, A. Petrone, T. Henderson, D. Ranasinghe, V.G. Zakrzewski, J. Gao, N. Rega, G. Zheng, W. Liang, M. Hada, M. Ehara, K. Toyota, R. Fukuda, J. Hasegawa, M. Ishida, T. Nakajima, Y. Honda, O. Kitao, H. Nakai, T. Vreven, K. Throssell, J.A. Montgomery Jr., J.E. Peralta, F. Ogliaro, M.J. Bearpark, J.J. Heyd, E.N. Brothers, K.N. Kudin, V.N. Staroverov, T.A. Keith, R. Kobayashi, J. Normand, K. Raghavachari, A.P. Rendell, J.C. Burant, S.S. Iyengar, J. Tomasi, M. Cossi, J.M. Millam, M. Klene, C. Adamo, R. Cammi, J.W. Ochterski, R. L. Martin, K. Morokuma, O. Farkas, J. B.Foresman, D. J. Fox, Gaussian Inc, Wallingford CT. Gaussian 16 Rev. C.01, 2016.
[59] R. Dennington, T.A. Keith, J.M. Millam, GaussView, Version 6, Semichem Inc., Shawnee Mission, KS, 2016.
[60] A.D. Becke, Density-functional thermochemistry. III. The role of exact exchange, J. Chem. Phys. 98 (1993) 5648–5652, https://doi.org/10.1063/1.464913.
[61] C. Lee, W. Yang, R.G. Parr, Development of the Colle-Salvetti correlation-energy formula into a functional of the electron density, Phys. Rev. B 37 (1988) 785–789, https://doi.org/10.1103/physrevb.37.785.
[62] Modern Theoretical Chemistry III, vol. 3 (1977) 1–28.
[63] P. Giannozzi, S. Baroni, N. Bonini, M. Calandra, R. Car, C. Cavazzoni, D. Ceresoli, G.L. Chiarotti, M. Cococcioni, I. Dabo, A. Dal Corso, S. Fabris, G. Fratesi, S. de Gironcoli, R. Gebauer, U. Gerstmann, C. Gougoussis, A. Kokalj, M. Lazzeri, L. Martin-Samos, N. Marzari, F. Mauri, R. Mazzarello, S. Paolini, A. Pasquarello, L. Paulatto, C. Sbraccia, S. Scandolo, G. Sclauzero, A.P. Seitsonen, A. Smogunov, P. Umari, R.M. Wentzcovitch, J. Phys.: Condens. Matter 21 (2009), 395502.
[64] P. Giannozzi, O. Andreussi, T. Brumme, O. Bunau, M. Buongiorno Nardelli, M. Calandra, R. Car, C. Cavazzoni, D. Ceresoli, M. Cococcioni, N. Colonna, I. Carnimeo, A. Dal Corso, S. de Gironcoli, P. Delugas, R. A. DiStasio Jr, A. Ferretti, A. Floris, G. Fratesi, G. Fugallo, R. Gebauer, U. Gerstmann, F. Giustino, T. Gorni, J Jia, M. Kawamura, H.-Y. Ko, A. Kokalj, E. Küçükbenli, M .Lazzeri, M. Marsili, N. Marzari, F. Mauri, N. L. Nguyen, H.-V. Nguyen, A. Otero-de-la-Roza, L. Paulatto, S. Poncé, D. Rocca, R. Sabatini, B. Santra, M. Schlipf, A. P. Seitsonen, A. Smogunov, I. Timrov, T. Thonhauser, P. Umari, N. Vast, X. Wu, S. Baroni, J. Phys.: Condens. Matter 29 (2017) 465901.
[65] M. Ernzerhof, G.E. Scuseria, Assessment of the Perdew-Burke-Ernzerhof exchange-correlation functional, J. Chem. Phys. 110 (11) (1990) 5029–5036, https://doi.org/10.1063/1.478401.
[66] S. Grimme, J. Antony, S. Ehrlich, H. A. Krieg, H. A consistent and accurate ab initio parametrization of density functional dispersion correction (DFT-D) for the 94 elements H-Pu. J. Chem. Phys. 132 (2010) 15. 10.1063/1.3382344.
[67] H. Li, Q. Zhang, C.C.R. Yap, B.K. Tay, T.H.T. Edwin, A. Olivier, D. Baillargeat, From bulk to monolayer MoS_2: evolution of Raman scattering, Adv. Funct. Mater. 22 (7) (2012) 1385–1390, https://doi.org/10.1002/adfm.201102111.
[68] É. Blanco, P. Afanasiev, G. Berhault, D. Uzio, S. Loridant, Resonance Raman spectroscopy as a probe of the crystallite size of MoS_2 nanoparticles, C. R. Chim. 19 (10) (2016) 1310–1314, https://doi.org/10.1016/j.crci.2015.08.014.
[69] S.K.S. Patel, K. Dewangan, S.K. Srivastav, N.K. Verma, P. Jena, A.K. Singh, N. S. Gajbhiye, Synthesis of α-MoO3 nanofibers for enhanced field-emission properties, Adv. Mater. Lett. 9 (8) (2018) 585–589, https://doi.org/10.5185/amlett.2018.2022.
[70] S.K.S. Patel, K. Dewangan, N.S. Gajbhiye, Synthesis and room temperature d0 ferromagnetic properties of α-MoO3 nanofibers, J. Mater. Sci. Technol. 31 (5) (2015) 453–457, https://doi.org/10.1016/J.JMST.2014.08.013.
[71] J.L. Zhen Ou, J. Campbell, D. Yao, W. Wlodarski, K. Kalantar-zadeh, In situ Raman spectroscopy of H2 Gas interaction with layered MoO3, J. Phys. Chem. C 115 (21) (2011) 10757–10763, https://doi.org/10.1021/jp202123a.